Switch-Mode Current Amplifier for Active Magnetic Bearings

Sergei Basovich, Tomer Ben-Moha, Mor Mordechai Peretz, Shai Arogeti, and Ziv Brand

Ben-Gurion University of the Negev, P.O.B 653 Beer-Sheva 84105, Israel, basovich@post.bgu.ac.il

***Abstract*—This paper presents the concept and the practical implementation of a switch-mode current amplifier for the use in Active Magnetic Bearings (AMB). The switch-mode amplifier consists of a full-bridge capable of operating in 2-level, 3-level or phase-shifted PWM mode. An optimal digital current-programmed mode controller lays out the foundations to a proximate-optimal, robust, large-signal dynamic response of the system under extreme cases of loading and parameters variations. In particular, the current amplifier developed is capable of following the desired reference for large inductance variations (due to displacement). The power stage combines a newly developed, efficient, passive-based current sensor that is capable of sensing bi-directional and near-zero currents, while being robust to external disturbances and maintaining simple and efficient structure. The presented current amplifier concept has been verified experimentally on a single-axis AMB platform using a dual channel amplifier prototype, controlled by a single 16 bit low-cost microcontroller.**

I. Introduction

The key factor that is required for reliable operation for Active Magnetic Bearings (AMB) is a well-regulated current-sourcing current amplifier with low quiescent noise to assure steady-state stability [1]. Another requirement is that the current amplifier is capable of sustaining large-signal load variations, and follow a desired reference with guaranteed dynamic performance under wide changes in the system parameters. The latter is due to the fact that the effective inductance of the actuator significantly varies with the displacement of the rotor [2],[3].

Two general types of current amplifiers exist in the literature in the context of AMB. One approach is based on the classic linear amplifiers, and it is inherently associated with very poor efficiency [4]. The more preferred approach to drive magnetic actuators is by switch-mode converters technology which has a proven superiority in terms of efficiency and reduced size at the cost of a larger, yet still acceptable, quiescent noise [5]. To further reduce the steady-state noise, a three-level PWM mode of operation is commonly used [2]. However, the controller implementation may become complex in particular when multiple actuators per control-axis are required.

Following the recent growth in popularity of digital control, adaptation of control concepts from motor drives and switch-mode power supplies (SMPS) applications that were applied to AMB systems, have demonstrated conceptual operation with good dynamic performance [6]. However, as in the initial steps in digital control of SMPS [7],[8] similar to analog control, operation is obtained using high-performance microprocessors which makes this type of solution economically-prohibitive, in particular for lower power AMB systems.

Another important element in the design of current-sourcing converter for AMB is the current sensor. Although the subject of current sensing has not been widely addressed hitherto, it is a key factor to assure the desired performance, especially for the case of switching systems. In [9], the actuator current is sensed via a series resistor, therefore introducing additional losses. These can be eliminated using a hall-effect device [10],[11], at the cost of sensitivity to external magnetic fields and more complex design. However, both methods exhibit poor SNR at lower current levels. Since the nonlinear AMB plants are usually controlled using the feedback linearization method [12], which involves the on-off switching of the opposite electromagnets, the capability of the proper near-zero currents sensing is crucial to the reliable AMB system operation. An alternative approach to current sensing derived from SMPS technology that is pursued in this study is using a current transformer. Here, the current of the switching element is passed via a pulse transformer and the full behavior of the signal is restored using additional circuitry. The main limitation of such design is associated with a reset of the pulse transformer [13].

The objective of this study is thus to introduce an efficient current amplifier for AMB applications with fully-integrated digital current-programmed mode controller and a newly developed digital-control-oriented current sensing method using a simple pulse transformer. The current amplifier for a 1-degree-of-freedom (DOF) AMB system (Fig.1) consists of two H-bridge converters, synchronously operating in a three-level PWM mode, governed and controlled by a single 16 bit, fixed-point, microcontroller. The amplifier was validated on a real AMB system, it exhibits robust response for changes in the reference, loading conditions and system parameters.

The paper is organized as follows; the current amplifier structure and principle of operation, as well as the description of the new current sensing method are given in Section II. The discrete optimal controller design is described in Section III. Section IV presents the experimental results, and Section V concludes the paper.

II. Current Amplifier Overview

A. Structure and Operating Principle

The switch-mode current amplifier (Fig.1) consists of eight MOSFETs, each four of them in H-bridge configuration, and

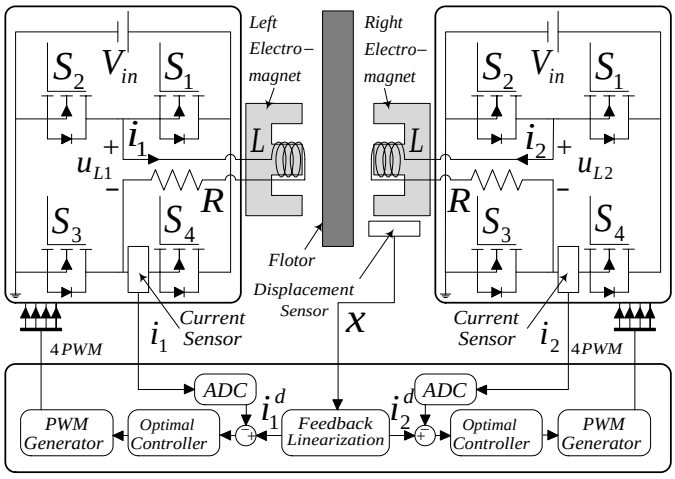

Figure 1: Structure of the two channel current amplifier for a 1-DOF AMB system

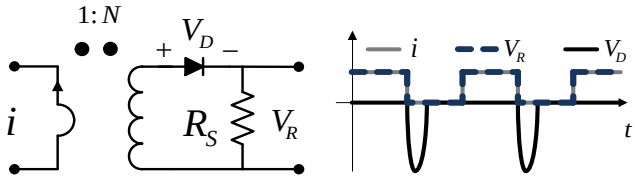

(a) Sensing circuit (b) Typical waveform

Figure 2: DC current transformer sensing

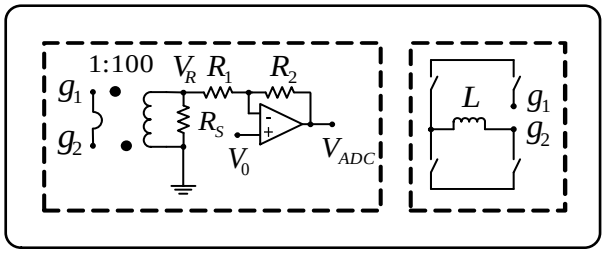

Figure 3: The introduced current sensor scheme

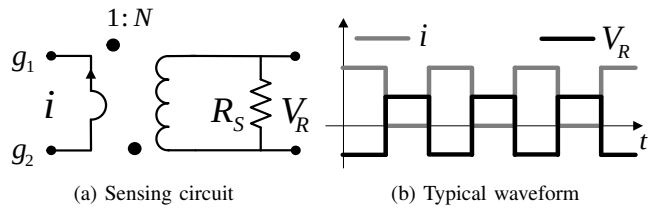

(a) Sensing circuit (b) Typical waveform

Figure 4: Introduced current transformer sensing

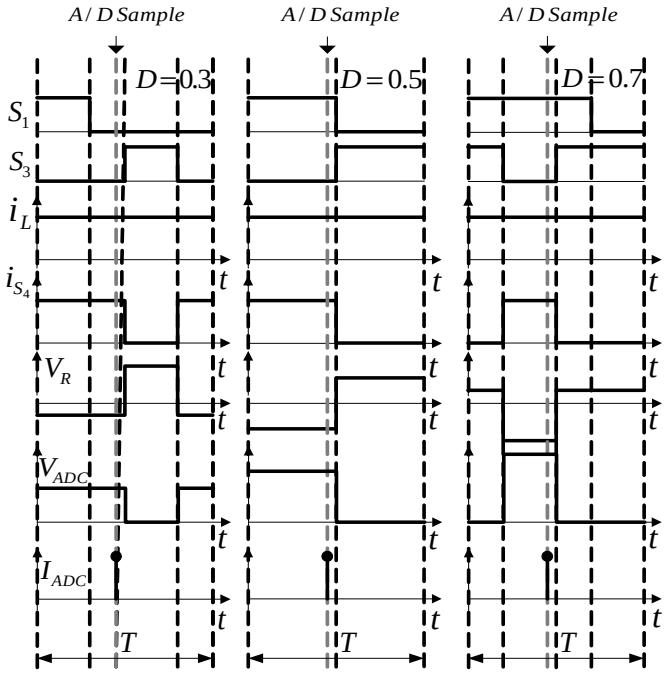

Figure 5: Current sensor operating principle for a variety of PWM signals (T is the sampling period, S_2 and S_4 are complimentary to S_1 and S_3 respectively)

a microcontroller capable of sampling voltage using A/D and generating 8 PWM signals.

According to schematic representation in Fig.1 a PC executing the feedback linearization based control law for an AMB receives the flotor displacement and calculates reference currents i_1^d, i_2^d for the amplifier control loop. The ADC of the microcontroller which is running the amplifier control loop samples the inductor current and reference current signals at a predefined rate, which in this study chosen to be at the switching frequency (upper bound of the switching system) to allow rapid response of the controller. The calculated error between the measured currents i_1, i_2 and i_1^d, i_2^d is then serves as an input to the optimal current-control algorithm developed to produce the required correction signal such to regulate the average actuator current PWM signals (S_1, S_2, S_3, S_4 where S_2,S_4 are complimentary to S_1,S_3 respectively) at the switching frequency of 100[kHz]. The PWM signals for two H-bridges are produced simultaneously using a dedicated per-converter PWM generator. The notation L, R, V_{in} is used to represent the actuator inductance, parasitic resistance and input voltage, respectively. The voltage between the actuator terminals in both H-bridges is denoted by u_{L1} and u_{L2}. As can be observed from Fig.1, the current regulation depends on the capability of accurately sensing actuator's current. To this end, a simple and efficient current sensor based on a pulse transformer, has been developed and is detailed in the following section.

B. Current Sensing Method

Accurate current measurement is essential to assure the desired closed-loop performance of the current amplifier. Similarly to inductor current sensing in SMPS, the main challenge in sensing the actuator's current, is the need to measure the DC component, which cannot be applied using simple current transformers. to this end, numerous current sensing methods for switch-mode applications have been covered in the literature, among them sense resistor [14], Hall-effect [15] and current transformers paired with signal reconstruction circuits [13]. However, in the context of AMB applications, the realization of current sensors has been conventionally applied by either resistive or Hall-effect concepts due to their capability to obtain both the AC and DC components of the signal. The main drawbacks of resistive measurement are the

introduction of additional losses in the conduction path, poor signal-to-noise ratio at lower currents, and that they require instrumentation with relatively high common-mode rejection ratio. Simple Hall-effect devices are prone drifts and are sensitive to external magnetic fields and nearby currents [15].

Current transformers are limited to AC measurements due to the need for flux balance (i.e. reset) to avoid saturation of the magnetic element. DC measurement via a transformer conventionally applies a reset circuitry, similar to the operation of a forward converter [13], i.e. the DC current is passed through the transformer in intervals sufficiently spaced to allow balancing of the flux. One possible implementation, widely used in SMPS applications (Fig.2) is to locate the primary winding of current transformer in series to a switching element and a diode in series to the measurement (on a resistor) at the secondary. In this way, the peak value of the pulsating current is accurately obtained during the conduction time of the switch and the reset of the transformer is facilitated during its off interval, however, the voltage developed at the secondary during the reset interval may be significantly high. By reversing the reset concept, another possible solution is the transformer-based current sense circuit that has been presented in [14] and further advanced in [16] for compatibility with digital control operation. There, DC current of the primary winding is obtained using an AC equivalent of the secondary winding. An external excitation in the secondary alternates the current, creating a pulsed waveform with peak current that is proportional to primary DC value. Assuming negligibly small ripple, a snapshot of the signal per sampling interval is sufficient data to reconstruct the actual current waveform. In addition to isolation, this method offers the possibility to directly measure the DC current through the actuator, however, it requires additional timing and control circuitry. Another drawback of both solutions in the context of AMB is the capability of measuring both positive and negative currents with the same fixture.

In this study, a modified approach, that combines the benefits of the above-mentioned current transformer based methods with the benefits of a digital control, has been developed. The description of the sensor and its principle of operation is assisted by Fig.3, Fig.4 and Fig.5.

As shown in Fig.4a, a conventional AC current transformer is realized to obtain the pulsating current shape of the switch current. The primary winding is connected in series to the switch and the current value is obtained on a resistor at the secondary. Since the original signal has a DC component, which is not passed through the transformer (Fig.4b), the relationship between the primary and the secondary peak currents depends on the duty ratio $(1-D)$ of the switch, and is expressed as:

$$i_{sec} = \frac{i_{avg} - i}{N} = \frac{-D\,i}{N}, \tag{1}$$

where i_{avg} is the DC component, N is the winding ratio of the transformer and D is the duty cycle of S_1 and S_3.

The operation of an AMB involves both positive and negative current through the actuator, depending on the duty ratio of the H-bridge. To allow acquisition of both negative and positive current values using an ADC, a fixed DC value, V_0, is added to the signal as can be observed in Fig.3. The sensed signal by the ADC, V_{ADC} can be expressed as:

$$V_{ADC} = \left(\frac{R_1+R_2}{R_1}\right) V_0 + \left(\frac{R_2}{R_1}\right) \frac{R_S}{N}\, D\, i \tag{2}$$

where R_S is the resistor on which the secondary current convert to voltage, R_1 and R_2 are the resistors that sets the gain of the amplifier.

Since the entire controller operation is facilitated digitally, the current duty ratio of all switches is available at all times. Given D, the real DC value of the actuators current can be obtained by:

$$i_{ADC} = \left[V_{ADC} - \left(\frac{R_1+R_2}{R_1}\right) V_0\right] \frac{R_1}{R_2}\frac{N}{R_S}\frac{1}{D} \tag{3}$$

which can be obtained using the ADC within the entire conduction time frame of the switch.

Fig.5 illustrates a detailed timing diagram and key waveforms of the introduced current sensor for various operating points of the current amplifier. Due to V_0 offset, the actuator current can be successfully restored for both negative (V_R>0) and positive (V_R<0) values. Using the current sensing method described here, the following advantages are obtained: no additional losses in the conduction path, galvanic isolation, simple realization without special instrumentation, EMI immunity, and lowered reset voltage compared to other solutions.

III. Control Design

The following section presents the control scheme for an 1DOF AMB actuator. The controller consists of two layers: the inner layer which regulates the AMB current, and the outer layer which controls the AMB flotor displacement.

A. Optimal Controller for Current Amplifier

This subsection is devoted to the optimal discrete controller design. In view of [17], the controller is designed for the regulation case. Following [18], the relation between the inductor voltage and current can be described by

$$\frac{di}{dt} + \frac{R}{L_n} i = \frac{u_L}{L_n} \tag{4}$$

where L_n is the nominal actuator inductance. Define the control signal u, as follows

$$u = 2D - 1, \quad -1 < u < 1 \tag{5}$$

Neglecting the switches on resistance and substituting (5) in (4) yields

$$\frac{di}{dt} + \frac{R}{L_n} i = \frac{V_{in}}{L_n} u \tag{6}$$

The following state variables

$$x_1 = \int_0^t i(\tau) d\tau, \quad x_2 = i \tag{7}$$

are used to obtain the state space representation of (6)

$$\dot{x} = Ax + Bu, \quad y = Cx \tag{8}$$

where $x \triangleq \{x_1, x_2\}^T$, and

$$A \triangleq \begin{bmatrix} 0 & 1 \\ 0 & -\frac{R}{L} \end{bmatrix}, \; B \triangleq \begin{bmatrix} 0 \\ -\frac{V_{in}}{L_n} \end{bmatrix}, \; C \triangleq \begin{bmatrix} 0 & 1 \end{bmatrix} \tag{9}$$

Assuming that the sampling period T is small with respect to the system bandwidth, the first order approximation can be

used to represent the system (8)-(9) in discrete state space by

$$x(k+1) = A_d x(k) + B_d u(k), \quad y(k) = Cx(k) \tag{10}$$

$$A_d \triangleq I + AT, \quad B_d \triangleq BT \tag{11}$$

where I is identity matrix. Applying the discrete linear quadratic regulation (LQR) methodology yields the control law of the form

$$u(k) = -Kx, \quad K = (B_d^T S B_d + R)^{-1} B^T S A_d \quad S, R > 0 \tag{12}$$

which minimizes the following cost function

$$J(u) = \sum_{n=1}^{\infty} (x(k)^T Q x(k) + u(k)^T R u(k)) \tag{13}$$

when $S > 0$ solves the algebraic Riccati equation

$$A_d^T S A_d + Q - S - A_d^T S B_d (B_d^T S B_d + R)^{-1} B^T S A_d = 0 \tag{14}$$

It can be verified that the following holds

$$rank\{B_d,\ A_d B_d\} = 2 \tag{15}$$

therefore a couple $\{A_d, B_d\}$ is controllable. Since a couple $\{A_d, C\}$ is not observable, in order to assure stability of (10)-(11) with (12) the weight matrix Q must be chosen in such a way that a couple $\{A_d, Q\}$ will be detectable [19]. In other words Q have to satisfy [20]

$$\exists P > 0 \quad | \quad A_d^T P A_d - P - Q^T Q < 0 \tag{16}$$

Thus, solving (14) for

$$Q = \begin{bmatrix} 2.3575e8 & 0 \\ 0 & 37 \end{bmatrix}, \quad R = 0.1 \tag{17}$$

one can obtain the following control gain

$$K = \begin{bmatrix} 3599.2 & 18 \end{bmatrix} \tag{18}$$

B. Feedback-linearization Controller for AMB

A 1-DOF AMB plant (Fig.6) was used in order to validate the presented power module. This AMB system consists of two electromagnets, a moving part, a static part and a proximity sensor. The moving part is connected to the static platform by a flexible link, the displacement of the moving part is measured by the proximity sensor. The moving part motion in the x direction can be described by a following equation

$$m\ddot{x} + kx = F \tag{19}$$

where m is the moving part equivalent mass, k is the moving part stiffness, and F is a force applied by electromagnets. This force can be modeled as [12]

$$F = F_1 - F_2 = c\frac{i_1^2}{(g_0 - x + x_f)^2} - c\frac{i_2^2}{(g_0 + x + x_f)^2} \tag{20}$$

where F_1 and F_2 are the forces applied by a left and right electromagnets respectively, c is the electromagnetic coefficient, g_0 is a nominal (corresponding to x=0) air gap, x_f is an additional length above the air gap due to a final permeability of the electromagnets core material, i_1 and i_2 are the control currents supplied to the left and right electromagnet respectively. The values of parameters for the employed in this study AMB system are given in Tab.I.

From (20) it can be observed that the force F is nonlinear in the moving part position x. To control the moving part

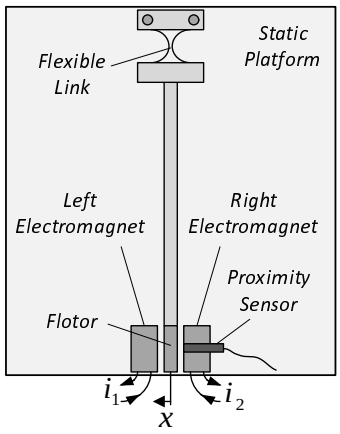

Figure 6: 1-DOF AMB system

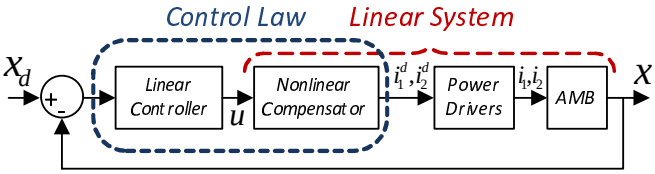

Figure 7: Feedback-linearization scheme

motion we use the feedback linearization technique. In general, this technique is based on a transformation of a nonlinear system to the linear one via feedback and a transformation of the state vector, and in this work we will use it to obtain a linearized expression for F (Fig.7). To this end, let us define the following transformation

$$i_1 = \begin{cases} (g_0 - x + x_f)\sqrt{um/c}, & u > 0 \\ 0, \quad otherwise \end{cases}$$
$$i_2 = \begin{cases} (g_0 + x + x_f)\sqrt{-um/c}, & u < 0 \\ 0, \quad otherwise \end{cases} \tag{21}$$

Transformation (21) means that the position of the moving part is controlled by switching between i_1 and i_2, i.e., a single control signal u is sufficient to carry out the regulation task. Substitution of (21) into (19)-(20) yields

$$\ddot{x} + \frac{k}{m}x = u \tag{22}$$

while for u we select the following PD control

$$u = -c_1(x - x_d) - c_2(\dot{x} - \dot{x}_d) \tag{23}$$

The Bode plot of the transference between $X_d(s)$ and $X(s)$ for

$$c_1 = 70000, \quad c_2 = 480 \tag{24}$$

is shown in Fig.8.

Table I: AMB Parameters

Parameter	*Description*	*Value*
m	Moving part equivalent mass	$0.48[kg]$
k	Flexible link stiffness	$1272.8[N/m]$
c	Electromagnetic coefficient	$3.73e-6[Nm^2/A^2]$
g_0	Nominal air gap	$313[\mu m]$
x_f	Add. length due to final permeab.	$1.8634[\mu m]$

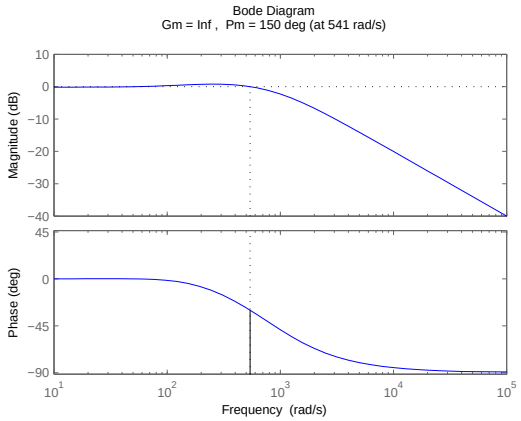

Figure 8: Transference for the closed loop system (22)-(23)

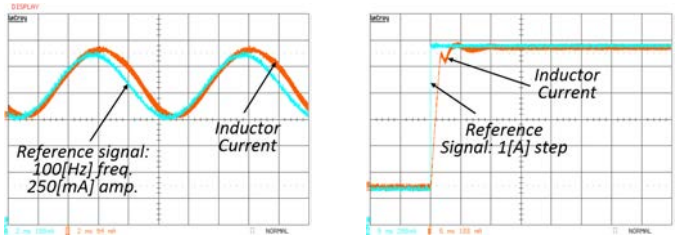

(a) Responce to sinusoidal signal (b) Step response

Figure 9: Tracking performance

IV. Experimental Results

The following section presents the experimental results conducted on the current amplifier. The first part presents the dynamic performance of the current amplifier prototype, when the second presents the dynamic performance of the 1 DOF AMB while driven by the current amplifier prototype.

A. Current Amplifier

The presented current amplifier concept has been experimentally validated by a prototype as described in Fig.1, operating at $100\,[\mathrm{kHz}]$. The system parameters were: $L = 17 - 45\,[\mathrm{mH}]$, $R = 1.6\,[\Omega]$, $V_{in} = 25\,[\mathrm{V}]$. The digital controller has been implemented with a single 16-bit, fixed-point, microcontroller that comprises a 10-bit ADC, and eight PWM outputs.

The current amplifier performance was validated for both set-point and sinusoidal wave tracking. The results of the experiments are shown in Fig.9a and Fig.9b. An experimental demonstration of the current sensing method is shown in Fig.10.

In order to evaluate the dynamic performance of the current amplifier (Fig.11), it should be noted that the relevant performance measure of the current amplifier should be obtained observing the response to a large-signal perturbation. Thus, the information available from the small-signal bode plot can lead to deceptive conclusions. On the other hand, the large-signal dynamic characteristics of the current amplifier can be estimated using the rise time of the response in Fig.9b as follows: $\omega_{BW} = 2/t_r$, where $\omega_{BW}\,[\mathrm{rad/sec}]$ is the equivalent bandwidth, and $t_r = 1.5 \times 10^{-3}\,[\mathrm{sec}]$ is the rise time.

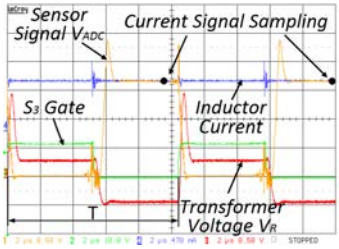

Figure 10: Sampling points within a single cycle

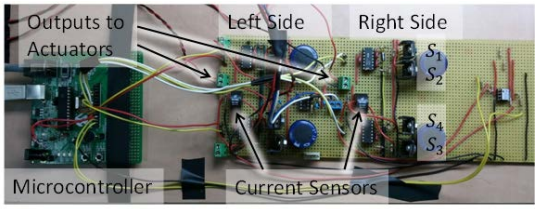

Figure 11: Power Amplifier

B. AMB System

The feasibility of the presented current amplifier was demonstrated using a real AMB system. (Fig.12). The outer control loop (AMB position regulation) was implemented using the MATLAB real-time toolbox and an acquisition card. The performed experiments include tracking the square wave reference signal and attenuation of $12[Hz]$ frequency vibration. In order to generate the vibration a DC motor with eccentric load (Fig.12) was attached to the moving part of the AMB system. The results of experiments for square wave tracking are shown in Fig.13, and the results for vibration attenuation are shown in Fig.14.

V. Conclusion

The AMB current amplifier with an effective current sensor was presented and implemented in this paper. The key idea behind the presented current sensing method is the sampling of a signal that caries information about the inductor current, instead of its full reconstruction. The experimental results indicates a satisfactory compliance of the current amplifier prototype with an AMB actuator.

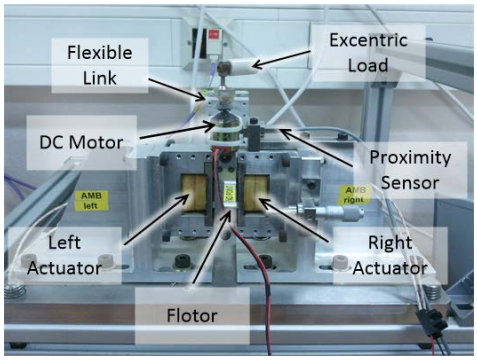

Figure 12: 1-DOF AMB Test Bed

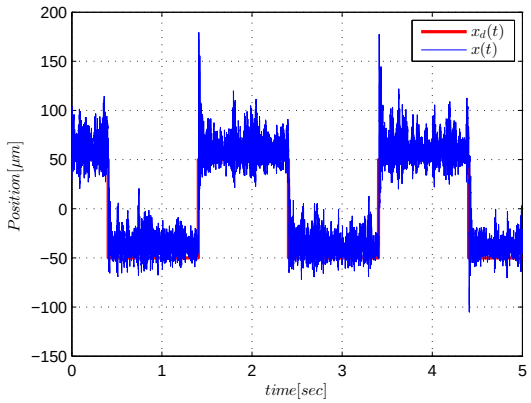

(a) AMB Position

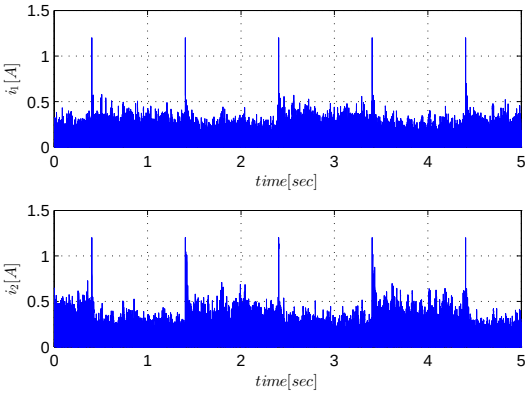

(b) Control Currents

Figure 13: Square wave tracking

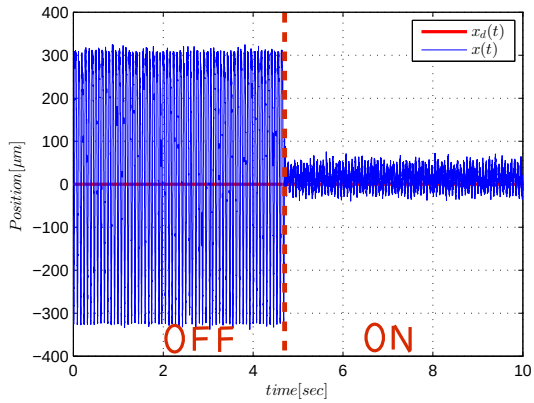

(a) AMB Position

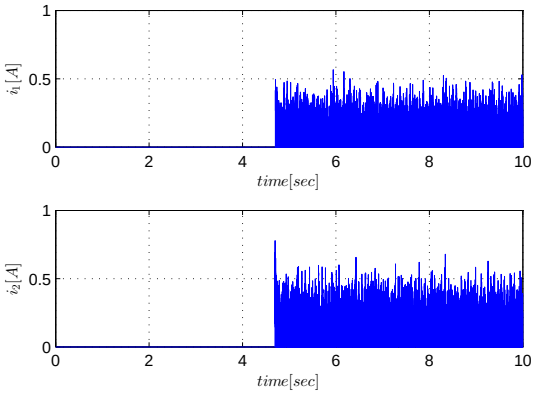

(b) Control Currents

Figure 14: Attenuation of 12[Hz] frequency vibration

REFERENCES

[1] G. Schweitzer and E. H. Maslen, *Magnetic Bearings Theory, Design and Applications to Rotating Machinery*. Springer-Verlag, 2009.

[2] J. Zhang and N. Karrer, "Igbt power amplifiers for active magnetic bearings of high speed milling spindles," in *Industrial Electronics, Control, and Instrumentation, 1995., Proceedings of the 1995 IEEE IECON 21st International Conference on*, vol. 1, 1995, pp. 596–601 vol.1.

[3] J. Y. Hung, N. G. Albritton, and F. Xia, "Nonlinear control of a magnetic bearing system," *Mechatronics*, vol. 13, no. 6, pp. 621 – 637, 2003. [Online]. Available: http://www.sciencedirect.com/science/article/pii/S095741580200034X

[4] J. Zhang and J. O. Schulze, "Synchronous three-level pwm power amplifier for magnetic bearings," in *International Symposium on Magnetic Bearings*, 1996.

[5] Z. Changsheng and M. Zhiwei, "A pwm based switching power amplifier for active magnetic bearings," in *Electrical Machines and Systems, 2005. ICEMS 2005. Proceedings of the Eighth International Conference on*, vol. 2, 2005, pp. 1563–1568.

[6] M. Peretz and S. Ben-Yaakov, "Time-domain design of digital compensators for pwm dc-dc converters," *Power Electronics, IEEE Transactions on*, vol. 27, no. 1, pp. 284–293, 2012.

[7] S. Lei and A. Palazzolo, "Real time digital control of magnetic bearings with microprocessors," in *Innovative Computing, Information and Control, 2006. ICICIC '06. First International Conference on*, vol. 2, 2006, pp. 154–157.

[8] W. Zhang, Y. Dun, Y. Sun, L. Yu, W. Shi, W. Zhang, and M. Shi, "High productivity reconfigurable digital control system and its application on magnetic bearing," in *Industrial Electronics and Applications, 2009. ICIEA 2009. 4th IEEE Conference on*, 2009, pp. 1844–1850.

[9] L. Zhang and J. Fang, "Pwm power amplifier with pd correction for magnetic suspending flywheel," vol. 5253, 2003, pp. 741–746. [Online]. Available: http://dx.doi.org/10.1117/12.521984

[10] L. Zhang, K. Liu, and X. Chen, "Fpga implementation of a three-level power amplifier for magnetic bearings," in *Electronic Measurement Instruments, 2009. ICEMI '09. 9th International Conference on*, 2009, pp. 1–455–1–460.

[11] A. Bonfitto, G. Botto, M. Chiaberge, L. Suarez, and A. Tonoli, "A multi-purpose control and power electronic architecture for active magnetic actuators," in *Power Electronics and Motion Control Conference (EPE/PEMC), 2012 15th International*, 2012, pp. DS2b.9–1–DS2b.9–5.

[12] D. Trumper, S. Olson, and P. Subrahmanyan, "Linearizing control of magnetic suspension systems," *Control Systems Technology, IEEE Transactions on*, vol. 5, no. 4, pp. 427 –438, jul 1997.

[13] R. W. Erickson and D. Maksimovic, *Fundamentals of Power Electronics (Second Edition)*, 2nd ed. Springer, 2001. [Online]. Available: http://www.worldcat.org/isbn/0792372700

[14] B. Mammano, "Current sensing solutions for power supply designers," Texas Instruments Incorparated, Tech. Rep., 2001.

[15] P. Ripka and A. Tipek, *Modern Sensors Handbook*. Wiley-ISTE, 2007.

[16] S. Ziegler, L. Borle, and H. H. C. Lu, "Transformer based dc current sensor for digitally controlled power supplies," in *AUPEC*, 2007.

[17] K. Ogata, *Modern Control Engineering (4th edition)*. Prentice-Hall, Inc. Upper Saddle River, New Jersey, 2002.

[18] J. Wang and L. Xu, "System model of three-level switching power amplifier for magnetic bearing," in *Measuring Technology and Mechatronics Automation, 2009. ICMTMA '09. International Conference on*, vol. 2, 2009, pp. 708–711.

[19] A. Locatelli, *Optimal Control An Introduction*. Birkhauser Basel, 2001.

[20] J. P. Hespanha, *Linear systems theory / Joao P. Hespanha*. Princeton University Press, 2009, formerly CIP.